The integrated intensity of the $g = 4$ signal was used to monitor the concentration of Mn(TPP)·I. The loss of intensity of the signal for I indicated the total concentration of Mn(TPP)·I and Mn(TPP)·2I. The concentrations of the two complexes were measured as a function of the concentration of I at constant concentrations of $Mn(TPP)ClO_4$. The data are consistent with the equilibria in (1) and (2) with $K_1 = 80 \pm 20\ M^{-1}$ and $K_2 = 120 \pm 40\ M^{-1}$.

$$Mn(TPP) + I \overset{K_1}{\rightleftharpoons} Mn(TPP)\cdot I \quad (1)$$

$$Mn(TPP)\cdot I + I \overset{K_2}{\rightleftharpoons} Mn(TPP)\cdot 2I \quad (2)$$

In a toluene solution containing spin-labeled pyridine, II, and $Mn(TPP)ClO_4$, there was competition between coordination through the nitroxyl oxygen and the pyridine nitrogen. In a solution with 2 mM II and 3 mM $Mn(TPP)ClO_4$, about 30% of the nitroxyl was coordinated to Mn(TPP) via the nitroxyl oxygen. This complex gave a six-line $g = 4$ signal similar to that observed for Mn(TPP)·I (Figure 1B). Thus, the presence of the substituent on the 4-position of the nitroxyl ring had little impact on the lineshape of the spectrum for Mn(TPP)·nitroxyl. When the pyridine nitrogen of II was bound to $Mn(TPP)ClO_4$, the nitroxyl signal was broad and overlapped the spectrum of II that was not coordinated ($g = 2$, not shown in Figure).

The five-membered ring nitroxyls III–VI also coordinated to $Mn(TPP)ClO_4$. The $g = 4$ signals in the EPR spectra of these complexes showed splitting (Figure 1C) that indicated the complex was not axially symmetric. Second-derivative spectra were recorded to improve the resolution of the spectra (Figure 1D). The hyperfine splitting pattern was simulated as two overlapping six-line patterns with slightly different g values and different nuclear hyperfine coupling constants. The values obtained for the spectra of Mn(TPP)·IV that are shown in parts C and D of Figure 1 were $g_1 = 4.014$, $a_1 = 86$ G and $g_2 = 3.990$, $a_2 = 115$ G. Similar parameters were obtained for the complexes with III, V, and VI. The largest variation was in the value of a_2, which ranged from 110 to 115 G. The similarities in the parameters for the five-membered nitroxyl, despite the variation in the nature of the substituents, suggested that the presence of a substituent on the 3-position of the nitroxyl ring was the dominant factor in causing the loss of axial symmetry. A nonaxial spectrum with differences in the manganese nuclear hyperfine splitting for the perpendicular components has also been observed for $Mn(TPP)(O_2)$ ($a_1 = 57$ G, $a_2 = 88$ G).[15]

These results indicate that EPR is a useful tool for examining nitroxyl complexes of metals with even numbers of unpaired electrons.

Acknowledgment. The partial support of this work by NIH Grant 21156 is gratefully acknowledged. Nitroxyls II and IV were prepared by Dr. B. M. Sawant (see ref 6). Nitroxyl V was prepared by Dr. J. K. More (see ref 7).

Registry No. I, 2564-83-2; II, 79991-43-8; III, 3229-73-0; IV, 79991-39-2; V, 81194-35-6; VI, 72444-16-7; $Mn(TPP)ClO_4$, 79408-54-1.

Contribution from the Department of Chemistry,
The Ohio State University, Columbus, Ohio 43210

Reaction Models for Cooperative Catalysis between Metal Ions and Acids or Bases: Hydration and Enolization of Oxalacetate

Suh-Jen Tsai and D. L. Leussing*

Received February 10, 1987

Investigations have been made of cocatalysis between Mg(II), Mn(II), and Zn(II) and the acid and base components of several buffers on the hydration and enolization rates of oxac. The results support preliminary conclusions[2] that complexing metal ion–general-base-cocatalyzed (or OH^--cocatalyzed) enolization processes of $oxac^{2-}$ closely conform to the Marcus function, eq 1, with the same intrinsic barrier, 13.5 kcal mol^{-1}, that is found for enolization in the absence of metal ions. Because of their ability to stabilize the charge developing on the keto oxygen atom as proton abstraction takes place, metal ions bound to $oxac^{2-}$ are even able to activate H_2O as a base catalyst. Stability constants of the intermediate enolate complexes evaluated by fitting the reaction rates to eq 1 are in good agreement with potentiometrically determined values in the case of Mg and Mn. The stability constant obtained for the Zn(II)–enolate by fitting the rate data is consistent with these other values and known trends of complex stabilities with different metal ions. General-acid-catalyzed enolization rates were examined in the context of reaction surfaces proposed in ref 20 and 21 for concerted reactions. The Guthrie surface, modified to conform to eq 1, was found to provide good quantitative agreement between predicted and observed rate constants for reaction paths assumed to involve a concerted reaction of 4-$Hoxac^-$ and the conjugate bases of the nominal general-acid catalysts. Complexed oxac also shows reaction along these same paths, but the models of the reaction surface indicate that the metal ion either partially, or completely, inhibits concerted proton transfer from the 4-CO_2H group. General-base-catalyzed hydration of $oxac^{2-}$ conforms to the modified Guthrie reaction surface. Metal ions increase general-base and OH^--promoted hydration rates owing to the formation of stable complexes with the OH^- addition product. A major solvent-catalyzed hydration pathway is proposed to proceed through a water dimer route. While complexing metal ions also show a prominent solvent-catalyzed pathway, the electrical field surrounding the metal ion may interfere with the water dimer mechanism, but an alternate route involving direct attack of H_2O on the keto carbon is possible.

Recent publications from our laboratory presented evidence that the Marcus function[1] (eq 1) accounts for metal ion rate enhancement observed for the enolization, hydration, and decarboxylation of oxalacetate[2] ($oxac^{2-}$) and the ketonization of enolpyruvate.[3] In eq 1, $\Delta G^{\ddagger}$ represents the actual activation barrier,

$$\Delta G^{\ddagger} = \Delta G^{\ddagger}_0 + \Delta G^{\circ}/2 + (\Delta G^{\circ})^2/16\Delta G^{\ddagger}_0 \quad (1)$$

which is related to the rate constant as given in eq 2; $\Delta G^{\ddagger}_0$ is the

$$\Delta G^{\ddagger} = -1.36 \log k + 17.4\ (25\ ^{\circ}C) \quad (2)$$

intrinsic barrier for the reaction and is the actual barrier when $\Delta G^{\circ} = 0$.

The initial observations indicated that for a given process $\Delta G^{\ddagger}_0$ remains unchanged when the reactants and products are complexed: if K_0 is the known equilibrium constant for the reaction of two uncomplexed ligands, A ⇌ B, and $\Delta G^{\ddagger}_0$ has been evaluated

(1) Marcus, R. A. *J. Phys. Chem.* **1968**, *72*, 891; *J. Am. Chem. Soc.* **1969**, *91*, 7224.
(2) Leussing, D. L.; Emly, M. *J. Am. Chem. Soc.* **1984**, *106*, 443–444.
(3) Miller, B. A.; Leussing, D. L. *J. Am. Chem. Soc.* **1985**, *107*, 7146.

0020-1669/87/1326-2620$01.50/0

from a measured rate, then the forward rate constant for the reaction of the complexes MA ⇌ MB is obtained from eq 1 by using the same $\Delta G^{\ddagger}_0$ and a ΔG° calculated from the modified equilibrium constant $K_M = K_0 K_{MB}/K_{MA}$ (K_{MA} and K_{MB} are the stability constants of MA and MB).

Decarboxylation,[4-6] base-catalyzed hydration,[2] and enolization[2,7-10] of oxac^{2-} result in the formation of carboxylates having an oxyanion substituted on the α-carbon atom (reactions Ia–c).

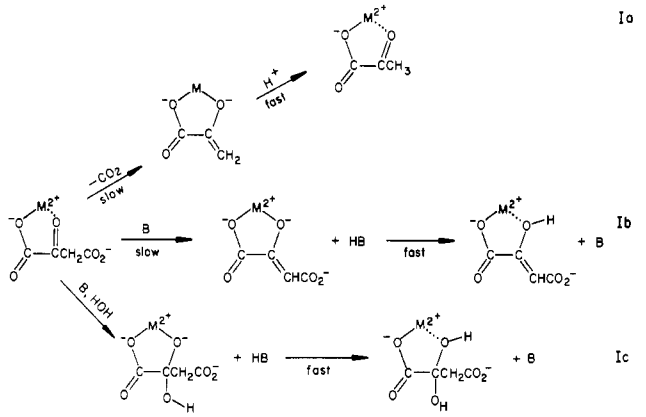

The high stabilities of the metal ion complexes of these chelates relative to the stability for the keto complex provides the additional driving force which increases the reaction rate. Equation 1 allows the quantification of these principles, which have been qualitatively recognized for some time.[4-6,10-18] In the case of enolization $\Delta G^{\ddagger}_0$ is little influenced by the nature of R and R′ in the carbonyl compound $RCH_2C(=O)R'$ so that $\Delta G^{\ddagger}_0$ may be approximated from the enolization rate of a carbonyl compound other than the one for which the metal ion effect is under consideration.[19] In addition to providing a means of predicting rate constants, conformity to eq 1 provides a means of sorting likely from unlikely reaction paths because ΔG° refers to the *rate-limiting step*. Because different reaction paths will, in principle, exhibit preequilibrium steps having different equilibrium constants, ΔG° can change from one path to another.

The observations originally reported dealt with the influence of Mg(II) on the enolization and hydration rates of oxac^{2-} in acetate and *N,N,N′,N′*-tetramethylethylenediamine (tetrameen) buffers[2] and the influence of Mg(II), Mn(II), and Cu(II) on enolpyruvate ketonization and oxac^{2-} decarboxylation rates.[3] In the present investigation the effects of Mg(II), Mn(II), and Zn(II) on hydration and enolization rates of oxac^{2-} in acetate, 3,3-dimethylglutarate (DMG^{2-}), 2-morpholinoethanesulfonate (MES^{-}), and *N,N*-bis(2-hydroxyethyl)glycine (bicine^{-}) buffers have been determined. The present investigations span a wider range of conditions than employed in the earlier studies and provide a more stringent test of the applicability of eq 1 to these reactions.

For some pathways (in principle all) proton transfer from solvent or buffer acid to the keto oxygen atom accompanies the primary reaction at the carbon center, and a description of progress over a second reaction coordinate is required to describe the transition state. The rate data acquired here were examined in the light of two models that generate reaction coordinate energy surfaces for concerted reactions. One model developed by Albery[19,20] had been found to account for cocatalysis by HOAc and OAc^{-} on the enolization rate of acetone.

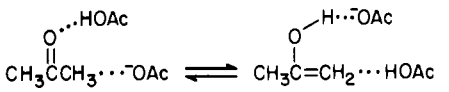

(II)

The second model was developed by Guthrie[21,22] to account for the effect of the strength of a general-base catalyst on rate constants for general-base-catalyzed additions to carbonyl groups, e.g. OH^{-} addition:

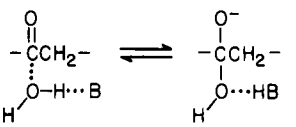

(III)

We have modified the Guthrie model to bring it into agreement with the Albery model for reactions that proceed along the peripheries of the surface. The examination of the rate data in the context of these surfaces provides valuable insight into possible reaction mechanisms.

Experimental Section

Rate determinations were performed in essentially the same manner as described earlier.[10] Biphasic absorbance changes were monitored as a function of time by using a stopped-flow apparatus in pH-increase and pH-decrease experiments in the presence or absence of metal ions (25 °C, I = 0.275). In pH-increase experiments, solutions of oxac at pH 1.4 were rapidly mixed with buffer solutions made sufficiently alkaline to neutralize the excess acid and give a mixed reaction solution having a specified higher pH within the buffer range of the weak acid. At pH 1.4 over half of the oxac is present as H_2oxac, which is substantially hydrated. When one or both protons are neutralized by raising the pH to 4.0 or higher, the hydrate content decreases and the keto and enol contents increase.[23,24] Changes in the enol concentration are followed by observing the absorbance changes in the near UV. The biphasic nature of these changes provides information regarding both tne enolization/ketonization and the hydration/dehydration rates.[23]

$$\text{hydrate} \underset{k'_{KH}}{\overset{k'_{HK}}{\rightleftharpoons}} \text{keto} \underset{k'_{EK}}{\overset{k'_{KE}}{\rightleftharpoons}} \text{enol} \qquad \text{(IV)}$$

In pH-decrease experiments, oxac solutions at pH 12.3 were mixed with acidic buffers to yield buffered reaction solutions having a lower pH. At pH 12.3 about 10% of the oxac is present as the enolate trianion, $^{-}O_2CC(O^{-})=CHCO_2^{-}$ (oxacH$_{-1}^{3-}$).[10] When the pH is decreased, the enolate is rapidly protonated and the excess enol relaxes primarily to the keto form. Equilibrium changes in the hydrate concentration are small (1–2%), and the absorbance–time curves appear to be monophasic; however, the neglect of processes involving the hydrate can lead to slight errors in the rate constants calculated for enolization/ketonization (see below).

Iso-pH rate measurements were performed by mixing buffered solutions of oxac^{2-} with solutions of a divalent metal ion in identical buffers. Complexation induces an increase in the enol content of oxac, which is followed spectrophotometrically. In all experiments performed in the presence of metal ions the distribution of oxac^{2-} between unprotonated, protonated, complexed, and uncomplexed forms was calculated by using the equilibrium constants given in Tables IA and III. Complexation of the metal ions by the buffer components was also taken into account. The computations were performed by using GENDIS, a program developed in our laboratory, which, for specified total concentrations, solves for the equilibrium concentrations of all species by using the Newton–Raphson iteration. In many of the experiments the concentration of complexing metal ion was so low that the fraction of oxac complexed was small; i.e., these experiments approached true catalytic conditions.

(4) Steinberger, R. A.; Westheimer, F. H. *J. Am. Chem. Soc.* **1951**, *73*, 429.
(5) Gelles, E.; Hay, R. W. *J. Chem. Soc.* **1958**, 3673.
(6) Gelles, E.; Salama, A. *J. Chem. Soc.* **1958**, 3683, 3689.
(7) Banks, B. E. *J. Chem. Soc.* **1961**, 5043; **1962**, 63.
(8) Bruice, P. Y.; Bruice, T. C. *J. Am. Chem. Soc.* **1978**, *100*, 4793.
(9) Bruice, P. Y. *J. Am. Chem. Soc.* **1983**, *105*, 4982.
(10) Emly, M.; Leussing, D. L. *J. Am. Chem. Soc.* **1981**, *103*, 628.
(11) Pederson, K. J. *Acta Chem. Scand.* **1948**, *2*, 252, 385.
(12) Pocker, Y.; Meany, J. E. *J. Phys. Chem.* **1970**, *74*, 1486.
(13) Prince, R. H.; Woolley, P. R. J. *J. Chem. Soc., Dalton Trans.* **1972**, 1548. Woolley, P. *J. Chem. Soc., Perkin Trans. 2* **1977**, 318.
(14) Schellenberger, A.; Hübner, G. *Chem. Ber.* **1965**, *98*, 1938.
(15) Breslow, R.; Fairweather, R.; Keana, J. *J. Am. Chem. Soc.* **1967**, *89*, 2135.
(16) Cox, B. *J. Am. Chem. Soc.* **1974**, *96*, 6823.
(17) Fife, T. H.; Squillacote, V. L. *J. Am. Chem. Soc.* **1977**, *99*, 3672.
(18) Groves, J. T.; Dias, R. M. *J. Am. Chem. Soc.* **1979**, *101*, 1033.
(19) Albery, W. J. *Annu. Rev. Phys. Chem.* **1980**, *31*, 227.
(20) Albery, W. J. *J. Chem. Soc., Faraday Trans. 1* **1982**, *78*, 1579.
(21) Guthrie, J. P. *J. Am. Chem. Soc.* **1980**, *102*, 5286.
(22) Lamaty, G.; Menut, C. *Pure Appl. Chem.* **1982**, *54*, 1837.
(23) Pogson, C. I.; Wolfe, R. G. *Biochem. Biophys. Res. Commun.* **1972**, *46*, 1048.
(24) Kokesh, F. C. *J. Org. Chem.* **1976**, *41*, 3593.

Table I. Equilibrium Constants

A. Oxalacetate: 25 °C, I = 0.275

L^{2-} = $^{-}O_2CC(=O)CH_2CO_2^-$

L_Σ = $^{-}O_2CC(=O)CH_2CO_2^-$ + $^{-}O_2CC(OH)=CHCO_2^-$ + $^{-}O_2CC(OH)_2CH_2CO_2^-$

reaction	log K	ref
$L_\Sigma^{2-} + H^+ \rightleftarrows HL_\Sigma^-$ (essentially 4-CO_2H)	3.9	*a*
$HL_\Sigma^- + H^+ \rightleftarrows H_2L_\Sigma$	2.7	*a*
$L^{2-} \rightleftarrows {}^{-}O_2CC(O^-)=CHCO_2^- + H^+$	−13.7	10
$L^{2-} \rightleftarrows {}^{-}O_2CC(OH)=CHCO_2^-$	−0.85	10
$^{-}O_2CC(OH)=CHCO_2^- \rightleftarrows {}^{-}O_2CC(O^-)=CHCO_2^- + H^+$	−12.3	10
$^{-}O_2CC(OH)=CHCO_2H \rightleftarrows {}^{-}O_2CC(OH)=CHCO_2^- + H^+$	−3.8	38
$^{-}O_2CC(OH)=CHCO_2H \rightleftarrows {}^{-}O_2CC(OH)=CHCO_2^- + H^+$	−3.7	*a*
$^{-}O_2CC(O^-)=CHCO_2H \rightleftarrows {}^{-}O_2CC(O^-)=CHCO_2^- + H^+$	7.0	*b*
$^{-}O_2CC(OH)_2CH_2CO_2^- \rightleftarrows {}^{-}O_2CC(O^-)(OH)CH_2CO_2^- + H^+$	−16.7	*b*
$L^{2-} + H_2O \rightleftarrows {}^{-}O_2CC(OH)_2CH_2CO_2^-$	−1.08	10
$^{-}O_2CC(=O)CH_2CO_2^- + OH^- \rightleftarrows {}^{-}O_2CC(O^-)(OH)CH_2CO_2^-$	−4.1	*c*
$^{-}O_2CC(OH)_2CH_2CO_2H \rightleftarrows {}^{-}O_2CC(OH)_2CH_2CO_2^- + H^+$	−4.5	*b*
$^{-}O_2CC(=O)CH_2CO_2^- + H_2O \rightleftarrows {}^{-}O_2CC(O^-)(OH)CH_2CO_2^- + H^+$	−17.8	*c*
$^{-}O_2CC(OH)(OH_2^+)CH_2CO_2^- \rightleftarrows {}^{-}O_2CC(OH)_2CH_2CO_2^- + H^+$	−0.3	*b*
$^{-}O_2CC(O^-)(OH_2^+)CH_2CO_2^- \rightleftarrows {}^{-}O_2CC(O^-)(OH)CH_2CO_2^- + H^+$	3.3	*b*

B. Cage Complex Formation: 25 °C, I = 0.275, d = 6 Å

$$A^n + B^m \overset{K_{cage}}{\rightleftharpoons} A^n\ B^m$$

product (*nm*)	6	4	3	2	1	0	−1	−2	−3
K_{cage}, M^{-1}	0.003	0.010	0.017	0.031	0.056	0.10	0.18	0.32	0.58

[a] This work, potentiometrically determined values. [b] Estimate based on the Taft parameters. [c] From the hydration ratio of $oxac^{2-}$ and an estimated pK_a based on the Taft parameters.

Table II. Forward Rate Constants for the Conversion of Keto Oxalacetate and Its Complexes to Hydrate and Enol at 25 °C and I = 0.275

A. Hydrate Formation

		log k^a obsd (calcd)			
catalyst	pK_a	$oxac^{2-}$	Mg(oxac)	Mn(oxac)	Zn(oxac)
H_3O^+	−1.7	2.73			
HOAc	4.53	−0.82			
H_2O	−1.7[b]	−1.58	−0.74	−0.36	−0.03
$bicine^-$	8.35[b]	−0.47	1.78 (2.0)		
OH^-	15.4[b]	2.70	5.46		6.89

B. Enolization

		log k^a obsd (calcd)			
catalyst	pK_a	$oxac^{2-}$	Mg(oxac)	Mn(oxac)	Zn(oxac)
		1. Acid Catalysis			
H_3O^+	−1.7	3.04 (3.9)	2.08		2.91
HOAc	4.53	0.23 (1.0)	0.04 (−0.81)	0.52 (−0.7)	0.90 (−0.4)
$HMES^\pm$	6.15	−0.21 (0.15)			
$HDMG^-$	6.67	−0.20 (−0.19)			
		2. Base Catalysis			
H_2O	−1.7[b]		−1.57 (−2.4)	−1.28 (−1.8)	−0.43 (−0.98)
^{-}OAc	4.53[b]		−0.11 (−0.32)	0.04 (0.20)	0.88 (0.95)
MES^-	6.15[b]		0.36 (0.56)	0.56 (1.1)	1.49 (1.8)
DMG^{2-}	6.67[b]		0.58 (0.51)	1.07 (0.95)	1.63 (1.8)
$bicine^-$	8.35[b]	−1.0	1.18 (1.70)		2.65 (2.9)
OH^-	15.4[b]	1.90	4.32 (4.6)		6.04 (5.6)

[a] The units of k are $M^{-1}\ s^{-1}$, except for H_2O as catalyst where k has the units of s^{-1}. [b] pK_a of conjugate acid.

In an earlier study[10] small discrepancies in enolization rate constants were obtained between pH-increase and pH-decrease experiments. These differences were found to be rooted in the failure of the assumption that the pH-decrease curves reflect only changes in enol content and could be treated as monophasic curves. In this study a new method of resolving the rate constants from the experimental absorbance–time curves was developed not only to remove these small differences but also to circumvent errors that may arise in experimental rate constants when the components of a biphasic curve have similar relaxation times or when one has a small amplitude compared to the other.

Evaluation of the Rate Constants

With reference to the coupled reaction set defined in eq IV, values of the forward and reverse rate constants are related through the equilibrium ratios [hydrate]′/[keto]′ = K'_{hyd} and [enol]′/[keto]′ = K'_{enol}. The primes indicate the sums over all complexed and uncomplexed forms.

Biphasic absorbance changes observed as the system approaches equilibrium are given by the expressions

$$A_t = A_\infty + A_1 \exp(-t/\tau_1) + A_2 \exp(-t/\tau_2) \quad (3a)$$

$$1/\tau_1,\ 1/\tau_2 = 0.5(S \pm (D^2 + 4P)^{1/2}) \quad (3b)$$

$$S = k'_{KE} + k'_{EK} + k'_{KH} + k'_{HK} \quad (3c)$$

$$D = k'_{KE} + k'_{EK} - (k'_{KH} + k'_{HK}) \quad (3d)$$

$$P = k'_{KE}k'_{KH} \quad (3e)$$

$$k'_{HK} = k'_{KH}/K'_{hyd} \quad (4a)$$

$$k'_{EK} = k'_{KE}/K'_{enol} \quad (4b)$$

Because low concentrations of metal ions were employed in the rate determinations the hydrate/keto and enol/keto ratios of these

Table III. Stability Constans of Metal Ion Complexes

$$M^{2+} + L^{l-} \overset{K_{ML}}{\rightleftharpoons} M(L)^{(2-l)+}$$

M(L)	log K_{ML}		
	Mg^{2+}	Mn^{2+}	Zn^{2+}
	3.8[a]	5.1[a]	7.0[a]
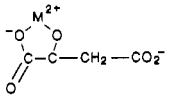	0.96[b]	1.41[b]	1.64[b]
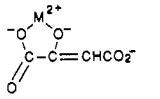	6.0[c], 5.9[b,d]	7.4[c], 7.0[d,e]	9.0[c]
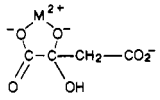	5.4[c]	6.6[c]	9.3[c]
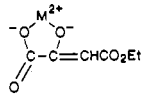	3.7[d,e]	4.5[d,e]	5.3[d,b]

[a] Reference 3. [b] Reference 38. [c] This work; from rate measurements and eq 1. [d] Potentiometric determination. [e] Reference 37. [f] Reference 50.

solutions approached those for free oxac, i.e. $K'_{hyd} \sim K_{hyd}$ and $K'_{enol} \sim K_{enol}$.

Forward rate constants for the disappearance of keto $oxac^{2-}$, k'_{KH} and k'_{KE}, can be expressed as the sums of the rates along parallel paths involving nominal catalysis by solvent, H^+, OH^-, and the buffer components HA and A (charges omitted to preserve generality)

$$k'_{KH} = (k^\circ_{KH} + k^H_{KH}[H^+] + k^{OH}_{KH}[OH^-] + k^{HA}_{KH}[HA] + k^A_{KH}[A])\alpha_K + (k^\circ_{MKH} + k^H_{MKH}[H^+] + k^{OH}_{MKH}[OH^-] + k^{HA}_{MKH}[HA] + k^A_{MKH}[A])\alpha_{MK} \quad (5)$$

$$k'_{KE} = (k^\circ_{KE} + k^H_{KE}[H^+] + k^{OH}_{KE}[OH^-] + k^{HA}_{KE}[HA] + k^A_{KE}[A])\alpha_K + (k^\circ_{MKE} + k^H_{MKE}[H^+] + k^{OH}_{MKE}[OH^-] + k^{HA}_{MKE}[HA] + k^A_{MKE}[A])\alpha_{MK} \quad (6)$$

The subscript KH represents the conversion keto → hydrate and KE represents keto → enol. Reversal of the subscript represents reaction in the opposite direction. An M in a subscript designates a constant pertaining to a metal ion complex. The fractions of oxac present as $oxac_{keto}^{2-}$ and $Moxac_{keto}$ are designated by α_K and α_{MK}.

Values of the individual rate constants for each of the terms appearing on the right-hand sides of eq 5 and 6 were obtained by simultaneously fitting an entire set of calculated to observed absorbance–time curves acquired in a series of experiments for a given buffer in which buffer ratios and concentrations were varied. Trial values of the rate constants were chosen, and eq 5 and 6 were used to calculate values of k'_{KH} and k'_{KE} pertinent to each experiment. Theoretical relaxation times for each experiment were calculated by using eq 3 and 4, and these were used to generate theoretical absorbance–time curves (eq 3a). The sum squares of the differences between each theoretical curve and the corresponding observed curve were calculated and these in turn were summed to obtain an overall sum square for the entire data set. The nonlinear curve-fitting program MINUIT[25] was used to adjust the rate constants so as to minimize the overall sum square. Experiments run in the absence of metal ions were analyzed first to evaluate the nominal rate constants for free oxac, and these results were then used to obtain the metal ion dependent rate

(25) James, F.; Roos, M. *Comput. Phys. Commun.* **1975**, *10*, 343.

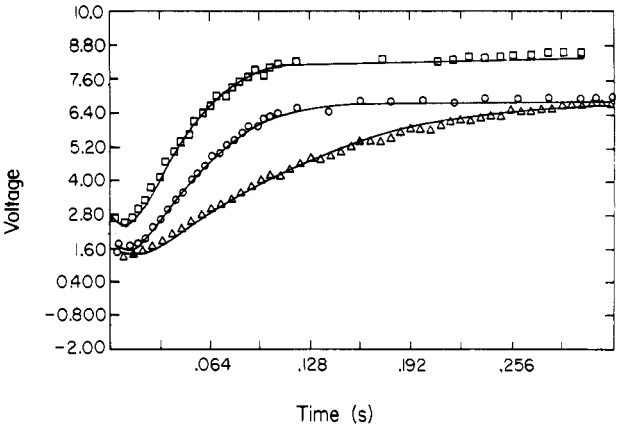

Figure 1. Voltage–time curves for pH-jump experiments with oxalacetate (pH initial 1.3; pH final 5.65; λ = 285 nm; 0.200 mM oxalacetate): (△) 25.0 mM MES; (○) 90. mM MES; (□) 150 mM MES.

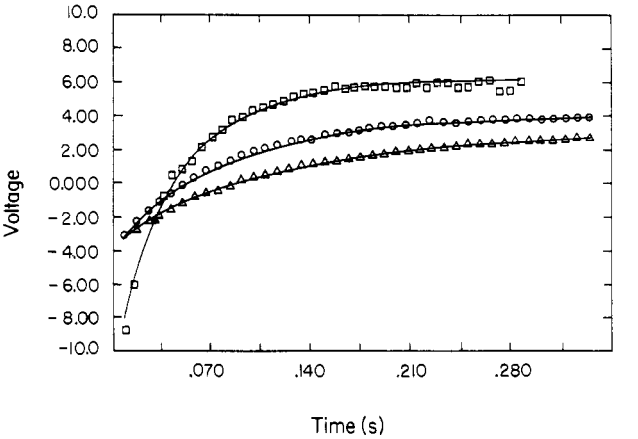

Figure 2. Voltage–time curves for pH jump experiments with oxalacetate in the presence of Zn(II) (pH initial 1.3; pH final 6.15; λ = 285 nm; 0.10 mM oxalacetate; 45.0 mM MES): (△) 0.500 mM Zn(II); (○) 1.00 mM Zn(II); (□) 5.00 mM Zn(II).

constants. Representative absorbance–time curves (actually voltage–time curves obtained from digitizing the spectrophotometric signal) and the "best" theoretical curves that fit them are shown in Figures 1 and 2. The values obtained for the nominal rate constants of eq 5 and 6 are given in Table II for all experiments.

The biphasic nature of the processes is quite evident in Figure 1. The sharp initial decrease in the signal denotes a decrease in the enol content as the protonated oxac is neutralized. Slower dehydration is accompanied by an increase in the enol content. In Figure 2 the biphasic behavior is less evident owing to a larger increase in the dehydration rate relative to the enolization/ketonization rates.

Computation of the Reaction Surfaces

Equation 1 implies that for reaction along a single coordinate, r, the free energy of the reactants (a) with a minimum at $r = 0$ is described by the parabolic function

$$\Delta G_{a,r} = 4(\Delta G^\ddagger_0)r^2 + \Delta G^\circ_a \quad (7)$$

and the free energy of the products (b) with a minimum at $r = 1$ is described by

$$\Delta G_{b,r} = 4\Delta G^\ddagger_0(1 - r)^2 + \Delta G^\circ_b \quad (8)$$

The transition state lies at the intersection of these two curves, and if the condition $\Delta G_{a,r} = \Delta G_{b(1-r)}$ is invoked, it can be shown that

$$r^\ddagger = (4\Delta G^\ddagger_0 + \Delta G^\circ)/8\Delta G^\ddagger_0 \quad (9a)$$

$$\Delta G^\circ = \Delta G^\circ_b - \Delta G^\circ_a \quad (9b)$$

and

$$\Delta G^{\ddagger} = 4\Delta G^{\ddagger}_0(r^{\ddagger})^2 + \Delta G^{\circ}_a \quad (10)$$

Equations 9 and 10 are alternate forms of eq 1.

When eq 1 or eq 9 and 10 are applied to second-order reactions, a correction to the free energies must be made for forming the reactant and product cage complexes

$$A + B \overset{K_{CR}}{\rightleftharpoons} A,B \overset{K_{rl}}{\rightleftharpoons} C,D \overset{1/K_{CP}}{\rightleftharpoons} C + D$$

If K_{eq} is the overall equilibrium constant for the reaction, $K_{eq} = [C][D]/[A][B]$, then the equilibrium constant for the rate-limiting step $K_{rl} = K_{eq}K_{CP}/K_{CR}$. The reduced forward rate constant is the quotient $k_{rl} = k_{obsd}/K_{CR}$. Any other fast equilibria occurring along the reaction path must also be taken into account in evaluating K_{rl} and k_{rl}.

Albery has taken 0.1 M^{-1} as the cage complex formation constant when one of the species is neutral and 1.0 when one is an H_2O molecule. We have adopted this same convention and have employed the Fuoss equation to correct for charge effects with the preexponential term set equal to 0.1 M^{-1} in order to be consistent with Albery's usage. The details are given more fully in ref 2. Values of the cage formation constants used here are given in Table IB.

When concerted reactions are encountered, it is useful to view the reaction progress along either a three-dimensional reaction surface or a two-dimensional reaction coordinate–energy contour map such as a More-O'Ferrall plot.[26] A perspective view of an Albery surface for general-acid–general-base-catalyzed enolization is shown in Figure 3. Transfer of a proton from a catalytic acid HA to the keto oxygen atom is depicted in the horizontal direction of the map, x, and the transfer of a $-CH_2-$ proton to a base B is depicted in the vertical direction, r. The reactions along the peripheries are the limiting reactions: (i) slow transfer of a $-CH_2-$ proton to base followed by fast transfer from HA to the 2-oxyanion; (ii) fast proton transfer from HA to the keto oxygen atom followed by slow transfer of a $-CH_2-$ proton to base (route V).

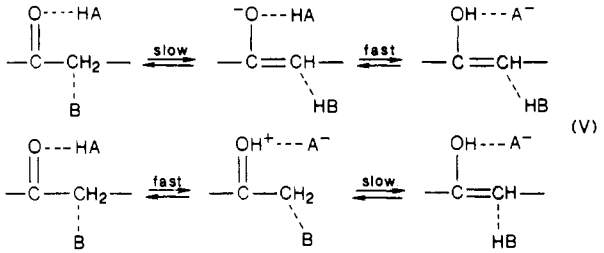

(V)

In Figure 3 the free energy of the reactant cage complex defines the height at the lower left-hand corner, a, and the free energy of the product cage complex defines the height at the upper right-hand corner, c. These species lie on the main reaction diagonal. The upper left-hand corner, b, and the lower right-hand corner, d, are defined by the energies of the species formed in the limiting reactions for acid catalysis: the enolate at b, and the oxonium ion at d. The free energies are expressed relative to the free energies of the nominal reactants taken as zero. When the free energy of d is high relative to b, then reaction proceeds along the periphery a → b → c. At low values of d relative to b the reaction proceeds along the periphery a → d → c. Intermediate values exist in which the transition state falls in the interior of the surface, indicating a concerted process in which, to varying degrees, reaction proceeds simultaneously along both reaction coordinates.

In general, the proton transfer to the oxygen atom is fast while the abstraction of a proton from a carbon atom is slow.[19,20,33-35]

In the Albery construction eq 7 and 8 are used to obtain the free energy profiles for the vertical processes with values of ΔG° for the left-hand and right-hand vertical axes, respectively, being given by the differences $\Delta G^{\circ}_b - \Delta G^{\circ}_a$ and $\Delta G^{\circ}_c - \Delta G^{\circ}_d$. The free energies of the interior points are obtained by assuming that the change in standard free energy for any vertical path is a linear function of the displacement in the horizontal direction. This assumption implies that proton transfer in the horizontal direction exhibits a negligible activation barrier. The free energy for a point at the coordinates r and x on the surface is calculated by using the equations

$$\Delta G^{\circ}_x = x(\Delta G^{\circ}_c - \Delta G^{\circ}_d) + (1 - x)(\Delta G^{\circ}_b - \Delta G^{\circ}_a) \quad (11a)$$

$$\Delta G_{rx} = 4(\Delta G^{\ddagger}_0)r^2 + (1 - x)\Delta G^{\circ}_a + x\Delta G^{\circ}_d \quad (11b)$$

reactant side of transition state ($r \leq r^{\ddagger}_x$)

$$\Delta G_{rx} = 4(\Delta G^{\ddagger}_0)r^2 + (1 - x)\Delta G^{\circ}_b + x\Delta G^{\circ}_c \quad (11c)$$

product side of transition state ($r > r^{\ddagger}_x$)

$$r^{\ddagger}_x = (4\Delta G^{\ddagger}_0 + \Delta G^{\circ}_x)/8\Delta G^{\ddagger}_0 \quad (11d)$$

along the ridge

The Albery surface possesses a ridge that connects the maxima lying on the vertical axes. This ridge defines the locus of the transition states, with the actual position being determined by the relative free energies of the corner species and the value of the intrinsic barrier. Under most conditions the transition state is located on one, or the other, of the vertical axes, but conditions exist under which it has an intermediate value, $0 < x < 1.0$. To see how this may occur, consider for simplicity, a surface for which $\Delta G^{\circ}_b \approx \Delta G^{\circ}_c$. If $\Delta G^{\circ}_a \ll \Delta G^{\circ}_d$, the transition state lies on the ab axis, and if $\Delta G^{\circ}_a \gg \Delta G^{\circ}_d$, the transition state lies on the dc axis. As ΔG°_a increases from the low value to the high one, a point is reached where the transition state crosses over from the left-hand axis to the right-hand one. This crossover is not sudden but spans a range in the values of the difference $\Delta G^{\circ}_d - \Delta G^{\circ}_a$. In the present example the crossover occurs in the vicinity $\Delta G^{\circ}_d - \Delta G^{\circ}_a \sim 0$.

The coordinates of the minimum on the ridge are given by

$$x^{\ddagger} = \alpha = [8\Delta G^{\ddagger}_0(\Delta G^{\circ}_a - \Delta G^{\circ}_d)/S - 4\Delta G^{\ddagger}_0 + \Delta G^{\circ}_a - \Delta G^{\circ}_b]/S \quad (12a)$$

$$S = \Delta G^{\circ}_a + \Delta G^{\circ}_c - \Delta G^{\circ}_b - \Delta G^{\circ}_d \quad (12b)$$

$$0 < x^{\ddagger} < 1 \qquad 0 < r^{\ddagger} < 1$$

and

$$\Delta G^{\ddagger}_{rx} = 4\Delta G^{\ddagger}_0(r^{\ddagger})^2 + (1 - x^{\ddagger})\Delta G^{\circ}_a + x^{\ddagger}\Delta G^{\circ}_d \quad (12c)$$

Hydration involves the addition of an OH^- to the carbonyl carbon atom. If H_2O is the reactant a proton transfer to base must also occur at some point along the reaction pathway. The limiting reactions are

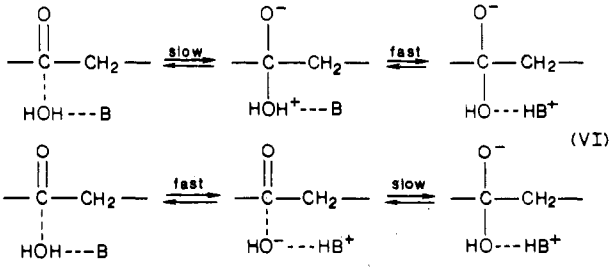

(VI)

In constructing the surface, fast proton transfer from an oxygen atom to a base is represented in the horizontal direction and slow addition of an oxygen atom to keto carbon is represented in the

(26) More-O'Ferrall, R. A. *J. Chem. Soc. B* **1970**, 274.
(27) Thornton, E. R. *J. Am. Chem. Soc.* **1967**, *89*, 2915.
(28) Jencks, W. P. *Chem. Rev.* **1972**, *72*, 705; **1985**, *85*, 511.
(29) Jencks, D. A.; Jencks, W. P. *J. Am. Chem. Soc.* **1977**, *99*, 7948.
(30) (a) Murdoch, J. R. *J. Am. Chem. Soc.* **1983**, *105*, 2660. (b) Donnella, J.; Murdoch, J. R. *Ibid.* **1984**, *106*, 2724. (c) Chen, M. Y.; Murdoch, J. R. *Ibid.* **1984**, *106*, 4735.
(31) Grunwald, E. *J. Am. Chem. Soc.* **1985**, *107*, 125.
(32) Pruszynski, P.; Chiang, Y.; Kresge, A. J.; Schepp, N. P.; Walsh, P. A. *J. Phys. Chem.* **1986**, *90*, 3760.
(33) Bell, R. P. *The Proton in Chemistry*, 2nd ed.; Cornell University Press: Ithaca, NY, 1973.
(34) Kresge, A. J. *Acc. Chem. Res.* **1975**, *8*, 354; *Chem. Soc. Rev.* **1973**, *2*, 475.
(35) Toullec, J. *Adv. Phys. Org. Chem.* **1982**, *18*, 1-77.

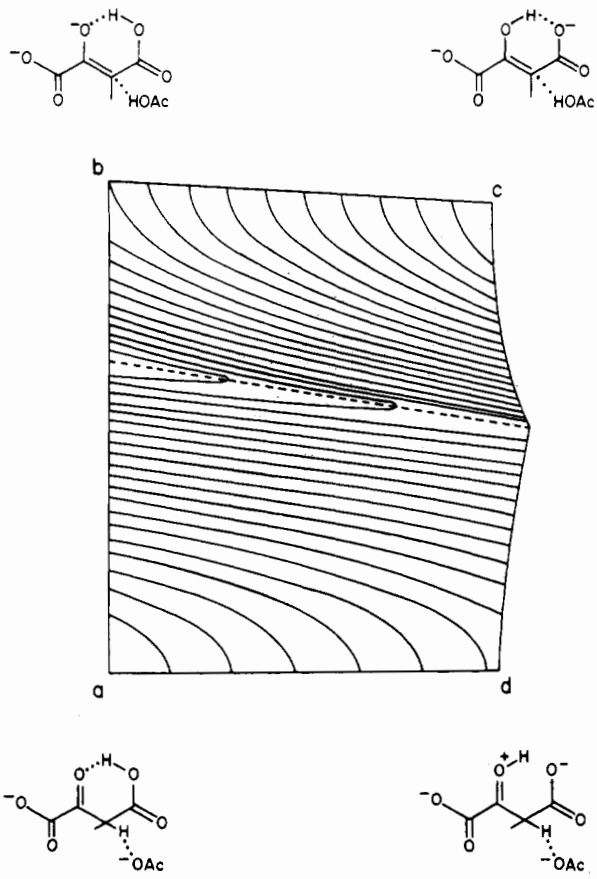

Figure 3. Perspective view of the Albery reaction surface for possible concerted catalysis in the enolization of oxalacetate. The viewer's eye is above the reactant corner at a. The products lie at c. The proton donor is the 4-CO_2H group of Hoxac$^-$ and the acceptor is $^-$OAc. The free energies of the corner species have been evaluated with respect to the free energy of the nominal reactants, HOAc and oxac^{2-}, taken as zero: $\Delta G°_a$ = 2.7 kcal mol^{-1}; $\Delta G°_b$ = 11.0 kcal mol^{-1}; $\Delta G°_c$ = 2.5 kc al mol^{-1}; $\Delta G°_d$ = 7.8 kcal mol^{-1} (pK_a^+ = 0.0). The maximum along the ab axis is 20.6 kcal mol^{-1}. The maximum along the dc axis 18.8 kcal mol^{-1}. The observed activation barrier is 17.1 kcal mol^{-1}. The contours lie at equal intervals of ≈0.9 kcal mol^{-1}. In order not to obscure the contours, the chosen view is high above point a. When one looks "due north" toward the gently downward sloping region at corner b, the peak along the left-hand axis does not extend above the horizon. When one looks toward the "northeast", the peak on the right-hand axis is seen to extend above the horizon even when it may be lower than the one on the left-hand axis.

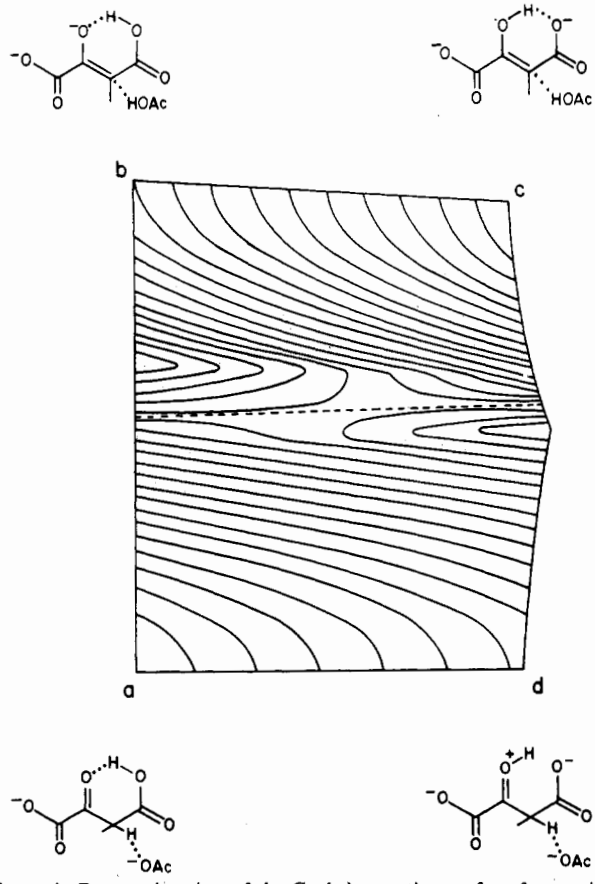

Figure 4. Perspective view of the Guthrie reaction surface for possible concerted catalysis in the enolization of oxac^{2-}. The reaction system is the same as that depicted in Figure 3. The crossover cleft, shown as the dashed line, lies at 16.1 kcal mol^{-1}. The observed activation barrier is 17.1 kcal mol^{-1}. See the legend of Figure 3 for comments on the perspective.

vertical direction. As is done in constructing the Albery surface, the energy profiles along each of the two vertical axes are generated by using an equation that describes the free energy as a function of reaction progress. Originally, Guthrie used an empirical function of the form, $ar^2 + br^3 + cr^4$, with the coefficients being evaluated from experimental data.[36] We have followed Albery's procedure and used the Marcus function to obtain these boundary free energy profiles. This modification reduces the number of parameters that need to be evaluated from experimental data and takes advantage of known values of the intrinsic barrier.

The Guthrie surface is completed simply by linearly interpolating in the horizontal direction between the energies lying on the vertical axes. In those systems where $\Delta G°_d > \Delta G°_a$ and $\Delta G°_b > \Delta G°_c$ the transition state on the left-hand axis occurs later than that on the right-hand axis. At some intermediate value of r the energies of the two curves are the same, creating a horizontal isoergonic contour. This contour falls at a value of r that is less than $r^‡$ on the left-hand axis but larger than $r^‡$ on the right-hand axis. Guthrie postulates that catalysis occurs when the reaction system proceeds from corner a toward corner b and crosses over from the left-hand axis to the right-hand axis along the isoergonic contour. By doing so, the reaction system is able to proceed from reactants at a to products at c having avoided both of the maxima.

Guthrie's concepts may also be applied to enolization, and in Figure 4 is shown a perspective view of a modified Guthrie reaction surface for the same system as depicted in Figure 3. It is seen in Figure 4 that the two axial peaks are not connected by a ridge, but are separated by a cleft. The catalytic reaction path, which is shown as the dashed line, follows the floor of the cleft.

Equation 7 describes the free energy along axis ab before the maximum is reached, and eq 13 describes the free energy along

$$\Delta G°_{cr} = 4\Delta G^‡_0(1 - r)^2 + \Delta G°_c \qquad (13)$$

the dc axis after the maximum has been passed. Equating (7) and (13) and rearranging yields the same result as expressed in eq 9a but now $\Delta G°$ is the difference $\Delta G°_c - \Delta G°_a$. Once $r^‡$ is obtained from (9a) the barrier height may then be calculated from (10).

The modified Guthrie surface differs from the Albery surface only in the way the interpolation to evaluate the interior points is made. The Albery surface possesses a higher interior barrier than the modified Guthrie surface, but both surfaces show the same peripheral characteristics. The Albery surface has been shown to account for the rate in a reaction where there is weak hydrogen bonding between two reactant molecules, e.g. between the carbonyl oxygen of acetone and HOAc as shown in eq III. The modified Guthrie surface, on the other hand, seems to furnish a better approximation of the barrier height in situations where the hydrogen bonding is stronger such as exists between an amine nitrogen atom and a solvent molecule in general-base-catalyzed addition of OH^- to a carbonyl group. Our results indicate that it also applies to those enolization reactions which involve an intramolecular hydrogen transfer. Obviously, either approach is an approximation to a much more complicated surface.

(36) Dunn, B. M. *Int. J. Chem. Kinet.* **1974**, *6*, 143.

Results and Discussion

Earlier an intrinsic barrier of 13.5 kcal mol^{-1} had been obtained for the general-base-catalyzed enolization/ketonization of oxac^{2-}, acetaldehyde, and pyruvate.[3] The presence in solution of complexing metal ions greatly accelerates these rates; nevertheless, the intrinsic barrier was found to be unchanged for the enolization of Mg(oxac) catalyzed by OH^- and tetrameen[2] and for the ketonization of enol pyruvate cocatalyzed by acetate and Mg(II), Mn(II), or Cu(II).[3] In the present investigation, bicine$^-$ was found to be the only base that, in the absence of complexing metal ions, showed sufficient catalytic activity to provide an accurate value of a second order rate constant. From $K_{rl} = 0.1/(0.031 \times 10^{-13.7+8.35}) = 1.4 \times 10^{-5}$ and a reduced rate constant $k_{rl} = 0.1/0.031 = 3.2\ s^{-1}$, $\Delta G^{\ddagger}_0$ is evaluated to be 13.2 kcal mol^{-1}, in excellent agreement with the earlier results. Bicine$^-$, therefore, is found to behave as a normal base catalyst and does not show the enhanced activity relative to the pK_a of its conjugate acid that has been observed with stronger tertiary amines.[8-10]

In contrast, cooperativity between metal ions and bases is strong enough that even H_2O serves as a base catalyst for the enolization of the weakest complex studied, Mg(oxac). Conformity to eq 1 was established by demonstrating that for each metal ion studied here a single enolate stability constant could be found that brings calculated rates into satisfactory agreement with the observed rates over the entire range of base catalysts, H_2O to OH^{1-}. The enolate stability constants obtained by fitting the data were found to be as follows: $10^{9.3}$ M^{-1}, Zn; $10^{7.4}$ M^{-1}, Mn; $10^{6.0}$ M^{-1} Mg [M^{2+} + oxac$H_{-1}^{3-} \rightleftarrows$ M(oxacH_{-1})$^-$]. Independently determined potentiometric values for the last two metal ions are in gratifying agreement with the kinetic results: $10^{7.0}$ M^{-1}, Mn; $10^{5.9}$ M^{-1}, Mg.[37,38] Unfortunately, a strong tendency for Zn(II) to form dinuclear enolate complexes has prevented the direct evaluation of the stability constant for the mononuclear enolate complex. The theoretical rate constants obtained by fitting the data are shown within parentheses in Table IIB2. The agreement with the observed values corresponds to a standard deviation of ±0.4 log units over a span of 9 log units (after converting the H_2O rate constants to second-order rate constants for purposes of comparing values having identical units).

As a further check for consistency, the stability constants for the oxacH_{-1}^{3-} enolate complexes can be compared in Table III to those reported earlier for the pyruvate enolate[3] and 4-ethyloxalacetate enolate[37] complexes. The inductive effect of the substituent on the 3-carbon atom is evident in the values: with reference to pyruvate enolate the 4-CO_2^- of oxac enolate brings about stability increases of 1.5–2 log units while the ester enolate stabilities show slight decreases. The constants for 4-Et(oxac)$^-$ were determined potentiometrically[37] and those for the other two ligands were calculated from reaction rates by using eq 1; nevertheless, all values are consistent with the structural differences between the ligands.

The rate law for oxac^{2-} enolization contains acid dependent terms that we have assigned nominally to catalysis by H_3O^+, HOAc, HMES$^{\pm}$, and HDMG$^-$. In analyzing the acetone rate data in the context of eq 1, Albery[20] has deduced that the rate observed for nominal HOAc-catalyzed enolization of acetone is too fast to arise from true catalysis by this acid as depicted in route VII. However, he did show that the rate is consistent with the

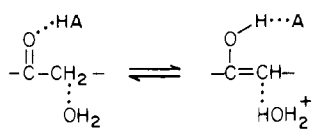

(VII)

kinetically equivalent reaction between the oxonium ion and acetate (route VIII).

Interpretation of the acid-dependent oxac rate data is complicated because there are three sites able to accept the proton. We have measured the pK_a of the 4-CO_2H proton to be 3.9; that

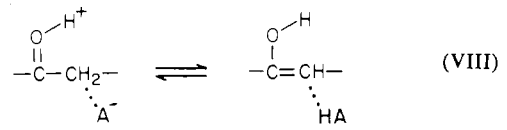

(VIII)

of the 1-CO_2H proton ($HO_2CC(=O)CH_2CO_2^- \rightleftarrows H^+ + {}^-O_2CC(=O)CH_2CO_2^-$) is estimated from the Taft parameters[39] to be 2.7, but pK_a^+ of the oxonium isomer ($^-O_2C(C=OH^+)$-$CH_2CO_2^- \rightleftarrows H^+ + {}^-O_2CC(=O)CH_2CO_2^-$) is highly uncertain. Estimates based on the Taft parameters place pK_a^+ about 3.6 units higher than that of the acetonium ion. Although there appears to be some consensus[40] that this latter value is −2.9, Hine[41] and Albery[20] present arguments in favor of more acidic values. While doubt exists as to the true value, it seems reasonable to assume that p$K_a^+ < 1.0$ for Hoxac$^-$.

In addition to paths VII and VIII, a third kinetically equivalent route involves transfer of a proton from the 4-CO_2H group to the keto oxygen atom concerted with transfer of the second proton to the conjugate base of the nominal acid catalyst (route IX). In

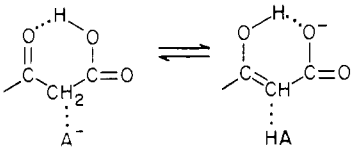

(IX)

studies on the enolization of keto acids, Bell and Fleundy[42,43] found that effective intramolecular catalysis can occur if a carboxylate, or carboxylic acid, on the same molecule can form a six-membered ring involving the carbon atom to which a proton is removed, or added. In contrast, other work[44] showed that the 1-CO_2H proton of pyruvic acid is an ineffective catalyst for enolization, presumably because of an unfavorable reaction geometry between the proton and an electron pair borne by the keto oxygen atom. For this reason, analogous paths involving the 1-CO_2H protomer of Hoxac$^-$ have not been considered here.

In the absence of an accurate value of pK_a^+ the strategy employed to test the applicability of the Albery model for concerted catalysis was to generate a number of surfaces with variable pK_a^+ (which influences the free energy of corner d of the contour map) to see if a value could be found that accounts for the observed rates. The Albery model allows only a limited range of pK_a^+ values over which a concerted process is possible. The corresponding range of ΔG°_d values for concerted reaction may be obtained from eq 14a,b and 15a–c.

$$\Delta G^\circ_{d,x=0} = [(\Delta G^\circ_a + \Delta G^\circ_c - \Delta G^\circ_b)Q - \Delta G^\circ_a]/(Q - 1) \quad (14a)$$

$$Q = (4\Delta G^{\ddagger}_0 - \Delta G^\circ_a + \Delta G^\circ_b)/8\Delta G^{\ddagger}_0 \quad (14b)$$

$\Delta G^\circ_{d,x=1}$ is the smaller root of the quadratic

$$(\Delta G^\circ_d)^2 + a_1\Delta G^\circ_d + a_2 = 0 \quad (15a)$$

$$a_1 = 4\Delta G^{\ddagger}_0 + \Delta G^\circ_b - \Delta G^\circ_a - 2\Delta G^\circ_c \quad (15b)$$

$$a_2 = -8(\Delta G^{\ddagger}_0)\Delta G^\circ_a + (4\Delta G^{\ddagger}_0 - \Delta G^\circ_a + \Delta G^\circ_b) \times (\Delta G^\circ_a + \Delta G^\circ_c - \Delta G^\circ_b) + (\Delta G^\circ_a + \Delta G^\circ_c - \Delta G^\circ_b)^2 \quad (15c)$$

The value of $\Delta G^\circ_{d,x=0}$ represents the lower limit which ΔG°_d can have and maintain the transition state on the left-hand axis. If ΔG°_d is lower than this value (d is more stable), the transition moves toward, or may lie on, the right-hand axis, but if ΔG°_d is higher than this value (d is less stable), the transition state remains on the left-hand axis. Conversely, $\Delta G^\circ_{d,x=1}$ represents the upper

(37) Biruš, M.; Leussing, D. L. *Inorg. Chem.* **1982**, *21*, 374.
(38) Emly, M., unpublished experiments.
(39) Perrin, D. D.; Dempsey, B.; Serjeant, E. P. *pK$_a$ Prediction for Organic Acids and Bases*, Chapman and Hall: New York, 1981.
(40) Stewart, R. *The Proton: Applications to Organic Chemistry*, Academic: New York, 1985.
(41) Hine, J. *J. Am. Chem. Soc.* **1971**, *93*, 3701.
(42) Bell, R. P. Fleundy, M. A. D. *Trans. Faraday Soc.* **1963**, *59*, 1623.
(43) Fleundy, M. A. D. *Trans. Faraday Soc.* **1963**, *59*, 1681.
(44) Bell, R. P.; Ridgewell, H. F. F. *Proc. R. Soc. London, A* **1967**, *298*, 178.

limit which $\Delta G°_d$ can have to maintain the transition state on the right-hand axis (preequilibrium transfer of a proton from HA to the keto oxygen atom). If $\Delta G°_d$ is higher than this value (d is less stable), the transition state shifts toward the left-hand axis. The derivations of eq 14a,b and 15a–c are provided in the Appendix.

It was found that route VII in which HOAc, $HDMG^-$ and $HMES^{\pm}$ are assumed to act simply as general-acid catalysts yield calculated activation barriers that are too high to account for the observed rates, supporting Albery's conclusions[20] regarding the HOAc dependent rate of acetone enolization. However, neither route VIII, which did account for the acetone/HOAc rate, nor route IX provided a satifactory fit to the $oxac^{2-}$ rate data. In constructing the Albery reaction surface for nominal HOAc catalysis via route IX (figure 3), a value of $pK_a^+ = 0.0$ was assumed. This value is above the range $-4 < pK_a < -1$ calculated for a concerted process to occur with ^-OAc as the base catalyst so that the lowest barrier falls along the d → c axis. Nevertheless, this barrier, 18.8 kcal mol^{-1}, is still higher than the observed value of 17.1 kcal mol^{-1}. An increase of pK_a^+ to 2.3 is required to bring the observed and calculated barriers into agreement.

Similar results were obtained for the remaining nominal acid catalysts. The pK_a^+ ranges predicted for concerted reactions increase with decreasing acid strength of the nominal catalysts. The ranges vary from −7.5 to −2.1 with H_3O^+ to −3.0 to 0.0 for $HDMG^-$, but in no case was a concerted reaction indicated. As was found with HOAc, the best agreement was obtained by assuming preequilibrium protonation of the keto oxygen atom (a → d → c). However, the values required of pK_a^+ to achieve the agreement between calculated and observed barriers on this periphery were found not only to be higher than the upper limit of 1.0 deduced above but were also dependent on the nature of the nominal acid catalyst (2.0, H_3O^+; 2.3, HOAc; 3.2, $HMES^{\pm}$; 4.0, $HDMG^-$). Reaction along either of the peripheral pathways should conform to eq 1 with a pathway via corner d of Figure 3 adhering to a single value of pK_a^+. The failure to do so suggests that a single-event transition state is inadequate to describe the rate behavior of these processes. In this regard, the Albery model fails to provide a satisfactory quantitative description of the observations.

Better results were obtained when the modified Guthrie model was applied to route IX. A perspective view of the surface derived for HOAc catalysis is shown in Figure 4. Here knowledge of the free energies of the species at corners b and d is not required to calculate the free energy of the cross-over contour, and a restriction that $pK_a^+ < 4.0$ is surely satisfied. The cleft seen lying between the axial peaks permits a Guthrie crossover at 16.1 kcal mol^{-1}. Although the agreement of this height with the observed barrier is only slightly better than given by the lowest barrier shown in Figure 3, the Guthrie model provides much better agreement over all of the nominal acid catalysts studied here. The predicted rate constants are shown in parentheses in Table IIB1. The calculated values for the weaker acid catalysts are seen to be in excellent agreement with those observed; however, with the stronger acid catalysts, the predictions are somewhat high. The difference is not very large considering the approximate nature of the models employed, but a true breakdown of the model appears to be exist, and tentatively, we attribute this to the presence of the barriers, which have been assumed to be negligible, for proton transfer to the keto oxygen. Nevertheless, the ability of the model to reproduce the catalytic rate constants determined here is sufficiently good to warrant considering its applicability to other reaction systems.

Enolization of the metal ion complexes is also subject to acid catalysis: H_3O^+ catalysis of Mg(oxac) and Zn(oxac) and HOAc catalysis of all three metal ion complexes were detected. It is expected that the interaction of a metal ion with the keto oxygen atom will inhibit protonation at this site, and in this light the relatively high rate constants are remarkable, as is also the fact that rates increase as the binding power of the metal ion increases, Mg < Mn < Zn. This pattern furnishes evidence that reactions between the conjugate bases of the nominal acid catalysts and

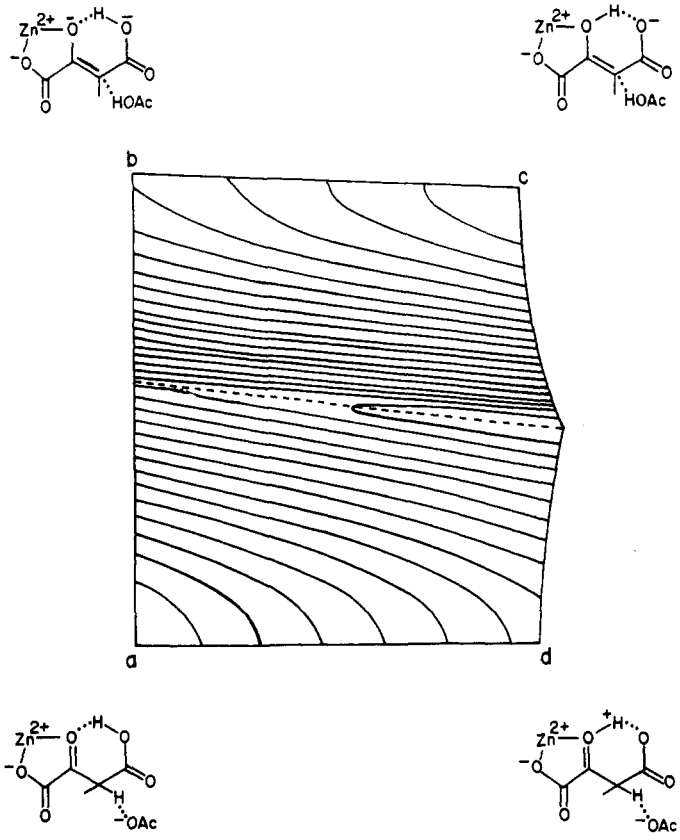

Figure 5. Perspective view of the Albery reaction surface for possible concerted catalysis in the enolization of Zn(oxac). The free energies of the corner species with respect to the nominal reactants, Zn(oxac) and HOAc, are as follows: $\Delta G°_a = 3.2$ kcal mol^{-1} ($pK_a = 3.0$); $\Delta G°_b = 5.4$ kcal mol^{-1}; $\Delta G°_c = 0.4$ kcal mol^{-1}; $\Delta G°_d = 10.1$ kcal mol^{-1} ($pK_a = -2.0$). The maximum along the ab axis is 17.8 kcal mol^{-1}. The maximum along the dc axis is 19.2 kcal mol^{-1}. The observed barrier is 17.1 kcal mol^{-1}. See the legend of Figure 3 for comments on the perspective.

the protonated complex are involved, $M(4\text{-Hoxac})^+ + A^- \rightarrow$ products.

Other evidence of a quantitative nature supports the suggestion that base catalysis is a feature of the mechanism. The ratios of the rate constants $k^{cat}_{ZnKE}/k^{cat}_{MgKE}$ are nearly the same for the nominal acid-catalyzed paths as for their conjugate bases: $k^{H}_{ZnKE}/k^{H}_{MgKE} = 7$ and $k^{H_2O}_{ZnKE}/k^{H_2O}_{MgKE} = 12$; $k^{HOAc}_{ZnKE}/k^{HOAc}_{MgKE} = 7$ and $k^{OAc}_{ZnKE}/k^{OAc}_{MgKE} = 10$. These near identities are not expected if a major component of the apparent acid-catalyzed reactions actually does involve proton catalysis because this component is absent in the base-catalyzed paths. However, the slightly smaller ratios shown by the nominal acid catalysts mildly suggest that a concerted proton transfer may also be a feature of the mechanism. If the carboxylate proton were in flight in the transition state, the effect of lowering the activation barrier would be greater with the weaker binding metal ion (Mg) than with the stronger binding metal ion (Zn) because protonation of the keto oxygen atom is easier with the former metal ion. Therefore, a concerted proton transfer should increase the reaction rate of Mg(oxac) more than that of Zn(oxac) as the figures indicate. However, the effect is seen to be small.

Additional insight may be gained by considering the reaction surface for a metal ion complex. To construct the surface it is necessary to know the stabilities of the protonated keto and enol complexes of oxac. Although little is known regarding these stabilities, by using resonable estimates it is possible to obtain a semiquantitative picture of the effect of the metal ion on the transition state. A perspective view of an Albery surface constructed for the enolization of Zn(oxac) nominally catalyzed by HOAc, but assumed to proceed via route IX, is shown in Figure 5.

The protonated metal ion complexes of oxac do not exhibit sufficiently high stabilities to have permitted a determination of

their stability constants by conventional means; therefore, assigning an upper limit of pK_a 3.0 to the 4-CO_2H proton of an M(4-Hoxac)$^+$ complex seems to be reasonable. Owing to the intervening saturated carbon atom between the 4-carboxylate group and the metal ion coordination site, it also does not seem likely that the pK_a falls much below this value. Therefore, pK_a = 3.0 was used in estimating the free energies of forming the assumed reactants from the nominal reactants at corner a. The stabilities of the protonated enolate complexes at corner b were taken to be the same as those of the 4-Etoxac$^-$ complexes (Table III). The free energy of the product enol complex at corner c was obtained from the experimentally determined values of the equilibrium constants for enolization $M(oxac)_{keto} \rightleftarrows M(oxac)_{enol}$: 5.7 for Zn(oxac), 1.0 for Mn(oxac), and 0.3 for Mg(oxac).[38] Thus, the free energies of the species at corners a–c relative to the free energy of the nominal reactants, M(oxac) and HOAc, can be placed with a fair degree of accuracy. Considerable doubt exists as to pK_a^+ of the protonated keto oxygen atom of complexed oxacH$^-$ at corner d, but the value should be lower than that of the uncomplexed ligand. In view of an upper limit of about 1.0 placed on pK_a^+ for uncomplexed oaxacH$^-$, an upper limit in the vicinity of −2.0 seems to be reasonable for Zn(4-Hoxac)$^+$. In Figure 5 it is seen that this value is sufficient to cause the transition state for enolization to fall on the left-hand axis. The affect of varying this value on the location of the transition state was also examined.

With respect to the surface for the free ligand (Figure 3), one effect of the metal ion is to slightly raise the free energy of the reactant at corner a, because protonating the 4-CO_2^- group of the complex is more difficult. In contrast, stabilization of the product enol complex causes the free energy at corner c to be lowered (Figure 5). These effects of a metal ion tend to cause the free energy of the transition state on the ab axis to increase slightly and that on the dc axis to decrease slightly, but in accordance with the Hammond postulate,[45] both transition states are shifted toward the reactant state. Inhibiting protonation at the keto oxygen atom raises the free energy at d and causes an increase in the transition state free energy, which counteracts the effect of the decrease at corner c. However, the position of the transition state is further shifted toward the reactant state.

More substantial effects are wrought by the metal ion in lowering the free energy at corner b. This is sufficient to effect a net decrease in the transition state free energy on the ab axis and cause an additional, and appreciable, shift of the position of the transition state toward the reactant state. Consistent with this predicted behavior, the data in Table II show a smaller dependence of the metal complex rate constants on the catalyst than is observed for the free ligand: replacing H_3O^+ as a nominal catalyst by HOAc results in a decrease in the rate constants of Zn(oxac) and Mg(oxac) by 2.0 log k units while the corrsponding effect on the rate constants for the free ligand amounts to 2.8 log k units. The surface drawn in Figure 5 shows that a Guthrie crossover is possible at 15.3 kcal mol^{-1} (log k = 1.5), but the dependence of the height of the transition state on the free energy of the species at corner b is inconsistent with this model. In the context of our hypothesis regarding the Albery and modified Guthrie surfaces, the metal ion is pictured to weaken the H bond between the 4-CO_2H proton and the keto oxygen atom so that the behavior of the reaction system adheres more closely to the Albery surface.

The concerted region on the Albery surface shown in Figure 5 is calculated to fall within the narrow region of pK_a^+ from 0 to −1.0. If $pK_a^+ > 0$, then reaction will proceed from a to c via corner d, and if $pK_a^+ < -1.0$, then the keto oxygen atom is too weakly basic to accept a proton in the transition state, and reaction proceeds via corner b. The barrier along this latter path is independent of pK_a^+, and establishes an upper limit on the rate constant. If pK_a^+ is sufficiently large to allow either a concerted or preequilibrium proton transfer, a faster rate will occur than is calculated for the route passing through corner b. For the Zn(4-Hoxac)$^+$/OAc$^-$ reaction depicted in Figure 5 the calculated activation barrier of 17.8 kcal mol^{-1} for the transition state on the ab axis yields a rate constant that is in fair agreement with the observed value, log k = −0.3 (calcd) and 0.9 (obsd). For the reactions of Mg(oxacH)$^+$ and Mn(oxacH)$^+$ along the same route, similar agreement is obtained. For Mg, log k = −0.8 (calcd) and 0.04 (obsd), and for Mn, log k = −0.7 (calcd) and 0.52 (obsd). For all of these metal ions the predicted rate constants are consistently low, but by assuming a concerted transfer of the 4-CO_2H proton, improved agreement between calculated and observed rate constants can be achieved. Because of the highly approximate nature of these calculations it is not possible to locate the position of the transition state with a high degree of confidence. Nevertheless, the calculations based on the properties of both surfaces indicate that a concerted proton transfer is a feature of the mechanism. In view of the influence of the metal ion on repressing pK_a^+, the transition state should lie much closer to the ab axis than is the case with the free ligand.

Hydration. The equilibrium hydrate/keto ratio of oxac^{2-} in aqueous solutions is 0.084 (25 °C). With the Taft parameters,[39] the pK_a of the diol is estimated to be 16.7, ($^-O_2CC(OH)_2CH_2CO_2^- \rightleftarrows {}^-O_2CC(O^-)(OH)CH_2CO_2^- + H^+$), and taking pK_w to be 13.7, the constant for OH$^-$ addition ($^-O_2CC(=O)CH_2CO_2^- + OH^- \rightleftarrows {}^-O_2CC(O^-)(OH)CH_2CO_2^-$) is calculated to be $10^{4.1}$ M^{-1}. The rates are dominated by OH$^-$ and H_2O catalysis. Of the buffers studied here only bicine$^-$ showed an appreciable effect on the rate. Earlier, catalysis by tetrameen was reported.[10] Except for the direct attack of OH$^-$ on the keto carbon, catalysis by general bases requires that at least one proton transfer accompany OH$^-$ addition, as shown in paths Ic and III.

Assuming that OH$^-$-catalyzed hydration does not involve a concerted proton transfer from H_2O, but simply involves the rate-limiting addition of the OH$^-$ to the keto carbon atom to give oxac·OH^{3-}, the equilibrium constant of $10^{-4.1}$ M^{-1} and the observed rate constant for $10^{2.7}$ M^{-1} s^{-1} yield an intrinsic barrier of 9.8 kcal mol^{-1}. The rate constants for bicine$^-$- and tetrameen-catalyzed hydration both yield values of 9.0 kcal mol^{-1} from the modified Guthrie equation. For the calculations described below we have taken an intermediate value of 9.5 kcal mol^{-1} as the intrinsic barrier for hydration.

Complexing metal ions accelerate pathways involving OH$^-$, general bases, and H_2O but turn off an H_3O^+-dependent route that is observed in acidic solutions with the free ligand. Analogous to the behavior deduced for enolization, metal ions appear to promote hydration rates by stabilizing the diolates, oxac·OH^{3-} (path Ic) and oxac·OH_2^{2-} (path XI), which are formed on OH$^-$ or H_2O addition to the keto carbon atom. Independent stability constants for the metal ion–oxac·OH^{3-} complexes are not known, so recourse was made to the same procedure as employed for analyzing the metal ion dependent enolate rates: stability constants were evaluated from the observed rates by using eq 1 and then examined for consistency with other results. Only the OH$^-$-dependent rates were subjected to this calculation because it was desired to examine the general-base-catalyzed rates separately in order not to obscure any differences that the metal ions might have on the proton transfer that accompanies these latter processes.

The hydrate complex stability constants were found to be similar to those of the corresponding enolates. The values of log K for the formation of the M(oxac·OH)$^-$ complexes are 9.3 (Zn), 6.6 (Mn), and 5.4 (Mg). The more basic 2-oxyanion of oxac·OH^{3-} acts to increase the interactions of the metal ions with this ligand relative to the enolate form of oxac, but this factor is offset by the absence of the ethylene double bond, which adds rigidity to the enolate chelate ring and provides a conduit for transmission of negative charge from the 4-CO_2^- group to the coordination site. Owing to these two opposing effects large differences in complex stabilities between the two ligands are neither expected nor observed.

Applied to bicine$^-$ cocatalysis the stability constant for the Mg(oxac) addition product leads to a predicted log rate constant of 2.0 for the hydration of Mg(oxac) from the modified Guthrie equation. This value lies in very good agreement with the experimental result of 1.78. Unfortunately, extensive complexation of Mn(II) and Zn(II) by the buffer together with solvent-dom-

(45) Hammond, G. S. *J. Am. Chem. Soc.* **1955**, *77*, 334.

inated rate terms has prevented acquiring accurate values of the rate constants for reaction of these metal ions along this pathway. Qualitatively, rate enhancements are observed.

Solvent-catalyzed hydration of $oxac^{2-}$ exhibits a relatively high rate constant, 0.026 s^{-1}. From values given in Table I, a rate constant of 5×10^{-4} s^{-1} is predicted for the direct addition of H_2O to $oxac^{1-}$ ($^-O_2CC(=O)CH_2CO_2^-$ + H_2O → $^-O_2CC(O^-)(OH_2^+)CH_2CO_2^-$), taking the equilibrium constant for OH^- addition to be $10^{-4.1}$ M^{-1} and pK_a = 3.3 for $^-O_2CC(O^-)(OH_2^+)CH_2CO_2^-$ ⇄ $^-O_2CC(O^-)(OH)CH_2CO_2^-$ + H^+. Williams, Schowen, and co-workers[46,47] have performed STO-3G computations on the hydration of formaldehyde in the gas phase and found that a pathway involving a water dimer provides a relatively low activation barrier.

(X)

It is claimed[46] that this pathway also accounts for the hydration rate constant of formaldehyde in aqueous solutions, 9.2 s^{-1}. Since the equilibrium hydrate/keto ratio of formaldehyde is 2.3×10^3, an apparent intrinsic barrier of 18.2 kcal mol^{-1} is calculated for this pathway. To the extent that this calculation is meaningful the excess of ~8 kcal mol^{-1} over the barrier for OH^- addition may be interpreted as arising from the two simultaneous proton transfers occurring in the transition state. In the context of eq 1 the solvent-catalyzed pathway for H_2O addition to $oxac^{2-}$ is remarkably consistent with formaldehyde hydration: the forward rate constant of 0.026 s^{-1} and the hydrate/keto ratio of 0.084 give an apparent intrinsic barrier of 18.8 kcal mol^{-1}. This close agreement with the formaldehyde result is strong evidence that both systems follow essentially the same mechanism, one that differs significantly from the mechanism for simple general-base-catalyzed hydration. Presumably this common mechanism involves the water dimer or one closely related to it.

Solvent-catalyzed hydration rates of the M(oxac) complexes are faster than the rates shown by free $oxac^{2-}$, but the metal ion has a far smaller influence than it exhibits along the base mediated pathways. In the case of Zn, as an example, the ratio $k^{OH}_{ZnKH}/k^{OH}_{KH}$ is > 10^4, but the ratio $k^{H_2O}_{ZnKH}/k^{H_2O}_{KH}$ is only 35. We interpret this difference as indicating that the metal ion interferes with one or both of the proton transfers along the water dimer route. It is known that electrostriction effects of divalent metal ions extend out to their third coordination sphere,[48,49] and solvent water molecules that can provide a dimer pathway between the oxygen and carbon atoms of the carbonyl group lie well within this distance of a metal ion bound to the keto oxygen atom. Orientation of these H_2O molecules with their oxygen atoms directed toward the metal ion rather than along the optimum proton transfer chain would strongly reduce the efficiency of this route.

It may not even be necessary for the water dimer mechanism to operate at all within the complex. A pathway in which the metal ion simply stabilizes the product of H_2O addition to $oxac^{2-}$ (path XI) appears to be feasible.

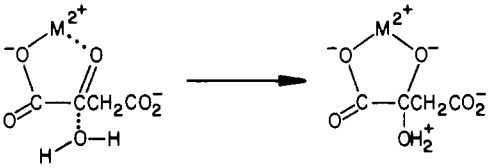

(XI)

For example in the case of Zn(II), taking $\Delta G^{\ddagger}_0$ to be 9.5 kcal mol^{-1}, from eq 1 $\Delta G°$ for path XI is calculated to be 13.4 kcal mol^{-1}. To satisfy this condition, the stability constant of the product Zn(II)–zwitterion complex need only be $10^{6.3}$ M^{-1}, a value 3 orders of magnitude lower than that for the complex formed through OH^- addition. Although there is not a known analogue against which to compare this result, the principal point to be made is that the product complex need not possess a high stability in order for the metal ion to promote the rate of H_2O addition. Any assistance from the 4-CO_2^- group by way of providing a concerted proton transfer from the attacking H_2O molecule would require even less stabilization by the metal ion.

Appendix

Derivations of Eq 14a,b and 15a–c. The free energies of points along the ridge are given by eq 11b using values of $r^{\ddagger}_x$ obtained from (11a) and (11d). The derivatives of these equations with respect to x are set equal to 0 ($x = x^{\ddagger}$), and the resulting equations rearranged to give (12a) and (12b), the solution for the value of $x^{\ddagger}$ at the minimum on the ridge. Equation 12c allows the minimum free energy to be calculated after $r^{\ddagger}_x$ and $x^{\ddagger}$ have been evaluated.

For a transition state on the left-hand axis $x^{\ddagger} = 0$. Setting the left-hand side of (12a) equal to 0 and solving for $\Delta G°_d$ lead to eq 14a,b.

For a transition state on the right-hand axis, $x = 1$. Setting the left-hand side of (12a) equal to 0, and solving for $\Delta G°_d$ results in the quadratic expressed by (15a) with the coefficients given by (15b) and (15c). Of the two roots only the smaller provides plausible values of pK_a^+ with the free energies for the species at corners a, b, and c encountered in this study. The larger root may represent a transition state in the "inversion" region of the Marcus function. We have not explored this possibility in detail.

Registry No. $^-O_2CCOCH_2CO_2^-$, 149-63-3; $^-O_2CC(OH)_2CH_2CO_2^-$, 60047-54-3; $^-O_2CC(OH)_2CH_2CO_2H$, 109151-20-4; $^-O_2CC(OH)=CHCO_2^-$, 7314-09-2; $^-O_2CC(OH)=CHCO_2H$, 109151-21-5; $^-O_2CC(O^-)=CHCO_2H$, 109151-22-6; $(HOCH_2CH_2)_2NCH_2CO_2^-$, 14047-36-0; H_3O^+, 13968-08-6; HOAc, 64-19-7; H_2O, 7732-18-5; OH^-, 14280-30-9; ^-OAc, 71-50-1; Zn^{2+}, 23713-49-7; Mn^{2+}, 16397-91-4; Mg^{2+}, 22537-22-0; $HMES^+$, 78693-72-8; $HDMG^-$, 109151-23-7; MES^-, 15417-07-9; DMG^{2-}, 20187-45-5.

(46) Williams, I. H.; Spangler, D.; Fernec, D. A.; Maggiora, G. M.; Schowen, R. L. *J. Am. Chem. Soc.* **1983**, *105*, 31.
(47) Williams, I. H.; Maggiora, G. M.; Schowen, R. L. *J. Am. Chem. Soc.* **1980**, *102*, 7831.
(48) Stranks, D. R. *Pure Appl. Chem.* **1974**, *38*, 303.
(49) Swaddle, T. *Adv. Inorg. Bioinorg. Mech.* **1983**, *2*, 103.